



Adsorption removal of Reactive Yellow 145 dye from aqueous solution using novel nZVI/(Fe–Mn) binary oxide/bentonite nanocomposite

Pham Van Lam, Nguyen Binh Duong, Phan Thi Ngoc Bich, Quan Thi Thu Trang*

Institute of Chemistry - Vietnam Academy of Sciences and Technology (VAST), 18 Hoang Quoc Viet Str. Hanoi, Vietnam, email: Quanthutrang5986@gmail.com (Q.T. Thu Trang), phamvanlam@ich.vast.vn (P.V. Lam), duongnguyentb1992@gmail.com (N.B. Duong), bich@ich.vast.vn (P.T.N. Bich)

Received 16 June 2022; Accepted 29 October 2022

ABSTRACT

A novel nanocomposite adsorbent of nZVI/(Fe–Mn) binary oxide/bentonite (IFMB) was developed in our study. In this paper, the adsorption behaviour of Reactive Yellow 145 (RY-145) dye from aqueous solution of IFMB was presented. The batch experimental results indicated that contact time, initial dye concentration and especially the initial pH value of the solution play important roles in the adsorption process of RY-145 onto IFMB. The adsorption efficiency was high and relatively stable in the range of pH < 7.0, when increasing the pH from 7.0 to 10.0, the adsorption efficiency decreased rapidly and at pH 11.0 there is almost not adsorption. The pseudo-second-order kinetics model was suitable for describing the adsorption kinetic data. The adsorption isotherm data was agreed well with the Langmuir model and the maximum adsorption capacity was as high as 338.9 mg·g⁻¹ at 30°C. In addition, IFMB could be easily regenerated by alkaline elution, and the adsorption efficiency after the fifth adsorption–desorption cycle was 74.5% of the one after the first adsorption–desorption cycle. These results suggested that IFMB is a promising candidate for azo dye wastewater treatment.

Keywords: nZVI/(Fe–Mn) binary oxide/bentonite; Novel nanocomposite; Reactive Yellow 145; Adsorption; Azo dyes

1. Introduction

Synthetic dyes have played an important role in modern life, commonly used in texture, printing, paper manufacturing, etc., approximately, 70% of all the dyes used in industry are azo dyes. They are characterized by the presence of one or more chromophoric azo groups (–N=N–) in their structure and the high physicochemical and microbiological stability [1–3]. The latter, an advantage in their use, is unfortunately a hindrance to their treatment in dye waste effluents. They are very difficult to remove by traditional conventional methods since their stability to light and oxidizing agents and resistance to aerobic digestion. A wide range of technologies has been developed for the removal of azo dyes from water and wastewater to decrease their

environmental impact and adsorption has gained tremendous popularity for its flexibility of design, ease of operation and low capital investment [4–6]. It has always been the goal of researchers to develop new effective adsorbents for the removal of dyes from wastewater.

Among the currently available adsorbents, iron oxides based nanomaterials are a group of emergent adsorbent for the removal of environmental pollutants from aqueous solutions because of their outstanding adsorption performance, low costs and eco-friendly properties [7–9]. Fe–Mn binary oxides (FMO) have been evaluated as the effective catalyst-adsorbents to remove pollutants from aqueous solutions. With its amorphous (or low crystalline) structure, FMO has a large specific surface area resulting in a high adsorption capacity. Studies have shown that FMO

* Corresponding author.

possesses the better adsorption and catalysis performance than either pure iron oxides or manganese oxides owing to their combination of the excellent adsorptive properties, high catalytic activity of iron oxide, high catalytic activity of manganese oxide and the highly effective recovery of the magnetic separation technique. FMO has been studied as an adsorption catalyst to remove As [10,11], heavy metals [12,13], organic dyes [9–14] from water. Zhong et al. [15] synthesized urchin-like Fe–Mn binary oxides with higher adsorption capacity for Cd(II). In the publish of Lu et al. [9], a nano-structured Fe–Mn binary oxide (nFMBO) was synthesized via a facile co-precipitation approach and showed high adsorption capacity for methylene blue.

In recent decades, nanometer-sized metallic iron, commonly known as nano zero-valent iron (nZVI), has become a popular material in environmental remediation with high reduction activity and adsorption capacity due to its small size, large specific surface area and strong reducing properties. The material exhibits a catalytic role in many processes, especially in the heterogeneous Fenton catalytic oxidation. They can also directly treat a wide variety of water pollutants including heavy metals, organic pollutants such as halogenated organic compounds (chlorinated hydrocarbons), dyes, etc. [16–18]. Nanocomposites of nZVI and the matrix such as polymers, some clay minerals, graphene, etc. have been extensively synthesized and studied. These carriers, not only increase the stability but also induce a uniform dispersion, reduce the aggregation of nZVI particles [16–22]. The application of nZVI particles on textile dye degradation is receiving more focus in the current decade. There have been many studies using nZVI or nZVI based on nanocomposites to directly treat different dyes as well as to catalyze other cleaning processes. Barreto-Rodrigues et al. [23] has optimized the synthesis conditions of nZVI from FeCl_2 and NaBH_4 , studied the degradation of disperse red 1 dye (DR1) and concluded that nZVI effectively decolorized DR1 in a short time but only affects the chromophore group ($-\text{N}=\text{N}-$) without mineralization. The latter occurs only by Fenton-like oxidation with the addition of H_2O_2 . Kerkez et al. [24] synthesized three composites of nZVI with three different clay minerals of commercial bentonite, kaolin and native clay also by reduction method with NaBH_4 in the presence of these clay minerals. All materials had the decolorization effect of RZ B-NG azo dye, but with a rather low efficiency of only 13.0%, 19.4%, 29.5% and 33.7%, respectively, for nZVI, nZVI on kaolin, nZVI on natural clay and nZVI on bentonite. The dye decolorization increased significantly with the addition of H_2O_2 (Fenton-like process), decolorization efficiency was about 92.0% and mineralization efficiency was 50.0%–58.0%.

The aim of our study is to develop a new adsorbent for the effective removal of azo dyes from aqueous solution. For this purpose, in our previous paper [25], nZVI/(Fe–Mn) binary oxide/bentonite nanocomposite (denoted as IFMB) was synthesized and its composition was optimized using response surface method (RSM), here the target function was the adsorption efficiency of Reactive Yellow 145 (RY-145) dye. Fe–Mn binary oxide and nZVI, both are good at the dye adsorption as discussed above. Combining the oxidation–adsorption catalytic ability of FMO binary oxide and

the catalytic reduction–adsorption property of nZVI in one material – IFMB, its dye adsorption capacity is therefore expected to enhance. Besides, we have used the exfoliated bentonite as a support for the dispersion and stabilization of nanoparticles in order to improve the applicability of the material in real wastewater treatment. In this sequel paper, the adsorption behaviour of IFMB for RY-145 dye, as the representative azo dye, was investigated.

2. Experimental

2.1. Materials

Reactive Yellow 145 dye (RY-145) is an anionic azo dye with chemical formula $\text{C}_{28}\text{H}_{20}\text{ClN}_9\text{Na}_4\text{O}_{16}\text{S}_5$ and its molecular structure is presented in Fig. 1.

RY-145 and other chemicals (NaOH , HCl , KMnO_4 , $\text{FeSO}_4 \cdot 7\text{H}_2\text{O}$, $\text{FeCl}_3 \cdot 6\text{H}_2\text{O}$, NaBH_4) are of analytical grade, purchased from Xilong Scientific Co., Ltd., (China).

Purified bentonite with about 20%–30% montmorillonite (given by supplier) was purchased from Minh Ha Bentonite Mineral JSC (Vietnam).

2.2. Preparation of IFMB

IFMB was synthesized as described in our previous paper [25]. Briefly, (Fe–Mn) binary oxide/bentonite composite (denoted as FMB) was firstly prepared by coprecipitation method following Zhang's publication [26]. The improvement was that Fe–Mn binary oxide is formed in an exfoliated bentonite suspension. And then, IFMB was formed by borohydride reduction of Fe(III) salts to nZVI in just prepared FMB suspension. The product was filtered and washed with deionized water (finally washed with ethanol to stabilize Fe^0 [27]). After drying by lyophilization method (temperature -60°C , pressure 200–300 mmHg) IFMB was obtained as dark brown solid.

IFMB was characterized by the methods of X-ray diffraction (XRD), energy-dispersive X-ray analysis (EDX) and nitrogen adsorption (using BET analysis). Point of zero charge (PZC) of the material was also determined in the previous paper [25]. Subsequently, in this paper, the morphology of prepared IFMB was examined by the field emission scanning electron microscope (FESEM, S4800-Hitachi).

2.3. Adsorption batch experiments

In the presence of oxygen dissolved in water, nZVI can be oxidized to Fe(II) and Fe(III) and lead to the formation of reactive oxygen species (e.g., $\cdot\text{OH}$ and $\cdot\text{O}_2^-$) via the Fenton-like reactions, which are able to decompose the dye [28,29]. Before adsorption experiments, the solutions were therefore aerated with Ar gas in 15 min in order to exclude nZVI oxidation and dye degradation caused by the presence of dissolved oxygen.

Generally, adsorption experiments were carried out at room temperature ($30^\circ\text{C} \pm 2^\circ\text{C}$) with an initial RY-145 concentration of $300 \text{ mg}\cdot\text{L}^{-1}$, IFMB dose of $1.0 \text{ g}\cdot\text{L}^{-1}$ at pH 6.0. The glass bottle of the mixture was placed on a IKA HS 260 basic shaker rotating at 120 rpm for 120 min. The pH was

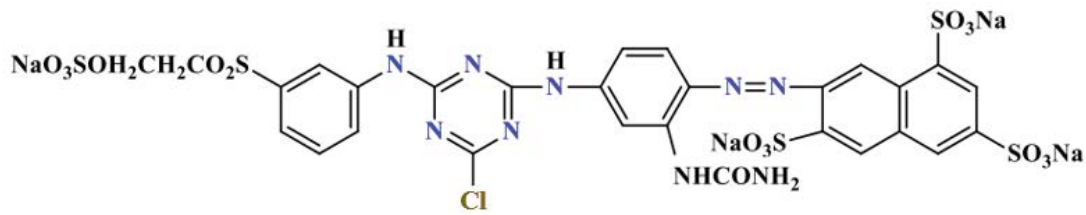


Fig. 1. Formula structure of RY-145.

adjusted by adding 0.1 M HCl or 0.1 M NaOH solution. After the experiments were completed, samples were filtrated through 0.2 μm cellulose acetate filter paper, the residual RY-145 concentration in solution determined using a UV-Vis spectrophotometer (UV/Vis Lambda 365) at $\lambda_{\text{max}} = 419 \text{ nm}$.

The influence of pH on the adsorption was studied within a pH range of 3.0–10.0 (IFMB is unstable in strong acidic medium (pH < 3.0)). Blank samples (without adsorbent) were similarly prepared to evaluate the effect of pH on the UV-Vis determination of the concentration of RY-145.

The adsorption kinetic experiments were performed with three materials, including IFMB, FMB and nZVIB. FMB has Fe/Mn molar ratio of 1.75 and nZVIB is nZVI/bentonite composite. Bentonite content is 9.56 wt.% in all three samples. The residual RY-145 concentration was analyzed at the given time intervals (0, 30, 60, 90, and 120 min). The kinetic data was analyzed by pseudo-first-order and pseudo-second-order kinetic models [30,31].

Linear pseudo-first-order equation:

$$\ln(q_e - q_t) = \ln q_e - k_1 t \quad (1)$$

Linear pseudo-second-order equation:

$$\frac{t}{q_t} = \frac{1}{k_2 q_e^2} + \frac{t}{q_e} \quad (2)$$

where q_t and q_e ($\text{mg}\cdot\text{g}^{-1}$) are the amount of RY-145 adsorbed per mass of IFMB (g) at time t (min) and at equilibrium, respectively; and k_1 (min^{-1}) and k_2 ($\text{g}(\text{mg}\cdot\text{min})^{-1}$) are the rate constants of the pseudo-first-order and pseudo-second-order models, respectively.

Adsorption isotherms were obtained with a range of RY-145 initial concentration of 200–900 $\text{mg}\cdot\text{g}^{-1}$. The Langmuir, Freundlich, and Dubinin–Radushkevich (D–R) adsorption isotherm models were used to describe equilibrium between IFMB and RY-145. The non-linear forms of these models can be expressed as in Eqs. (3)–(5) [31,32].

Langmuir model:

$$q_e = \frac{Q_{\text{max}} K_L C_e}{1 + K_L C_e} \quad (3)$$

Freundlich model:

$$q_e = K_F (C_e)^{1/n} \quad (4)$$

Dubinin–Radushkevich model:

$$q_e = (Q_{\text{max}}) \exp(-K_{\text{DR}} \varepsilon^2) \quad (5)$$

where C_e ($\text{mg}\cdot\text{L}^{-1}$) and q_e ($\text{mg}\cdot\text{g}^{-1}$) is RY-145 concentration in solution and the amount of RY-145 adsorbed per mass of IFMB (g) at equilibrium, respectively, Q_{max} ($\text{mg}\cdot\text{g}^{-1}$) is the maximum monolayer adsorption capacity of IFMB, K_L ($\text{L}\cdot\text{mg}^{-1}$) is the Langmuir constant describing adsorption affinity for the adsorbent, K_F ($\text{mg}\cdot\text{g}^{-1}(\text{L}\cdot\text{mg}^{-1})^{-1/n}$) and n (dimensionless) are the Freundlich constants representing adsorption capacity and intensity of adsorption, respectively, K_{DR} ($\text{mol}^2\cdot\text{kJ}^{-2}$) is the constant related to the adsorption energy and ε ($\text{kJ}\cdot\text{mol}^{-1}$) is the adsorption potential.

RY-145 removal efficiency was calculated according to Eq. (6) where R is RY-145 removal efficiency, C_0 and C_t ($\text{mg}\cdot\text{L}^{-1}$) are RY-145 concentration in solution at zero time and t time, respectively.

$$R(\%) = \frac{C_0 - C_t}{C_0} \times 100 \quad (6)$$

2.4. Regeneration experiment

Amount of 500 mL of 300 $\text{mg}\cdot\text{L}^{-1}$ RY-145 solution and 0.5 g of IFMB were placed in a 1,000 mL beaker and stirred at 120 rpm and room temperature for 120 min. The solution was filtered and RY-145 concentration was determined. IFMB separated from the solution was eluted with 0.1 M NaOH solution until the dye was completely desorbed. IFMB was then washed with distilled water to neutral pH and washed several times with ethanol to protect the Fe^0 composition in the material [27]. After drying at 80°C, the first time adsorbed IFMB was obtained and used continuously in the following cycles. The adsorption–desorption cycle was repeated 5 times. The removal efficiency of RY-145 in each cycle was calculated according to Eq. (6).

Determination of the loss of RY-145 in a closed adsorption–desorption cycle: The mixture of 100 mL of RY-145 solution ($C_0 = 300 \text{ mg}\cdot\text{L}^{-1}$, aerated with nitrogen for 15 min) and 0.3 g of IFMB was shaken at 120 rpm for 120 min. Desorption was then performed by adjusting making up the suspension to 200 mL with distilled water and stirring for 60 min. Solution was filtered and RY-145 concentration was determined by UV-Vis method.

XRD patterns of IFMB samples, as prepared and after 5 cycles, were also recorded.

3. Results and discussion

3.1. Characterizations of IFMB

Characterizations of IFMB material were determined in the previous paper [25]:

- The composition (calculated from the composition of initial materials, wt.%): Bentonite 9.56, nZVI 16.97, and Fe–Mn complex oxide (FMO, Fe/Mn molar ratio of 1.75) 73.74;
- The phase characterization: nZVI particles exist in crystalline form, the Fe oxide and Mn oxide of the Fe–Mn binary oxide are mainly amorphous and bentonite is in exfoliated form;
- The specific surface area (BET): $218 \text{ m}^2\cdot\text{g}^{-1}$;
- PZC: 6.76.

Scanning electron microscopy (SEM) images of exfoliated bentonite, FMB and the just prepared IFMB samples are given in Fig. 2. It can be seen from the image of FMB that amorphous FMB was likely obtained as a porous coating on the surface of bentonite. The surface of IFMB is obvious different with nearly spherical Fe⁰ nanoparticles, which are relatively uniform in size of only about 10 nm.

3.2. Effect of pH and supposed mechanism of RY-145 removal by IFMB

The effect of pH on the adsorption efficiency of RY-145 is illustrated in Fig. 3. When the pH increased from 3.0 to

about 7.0, the adsorption efficiency decreased insignificantly (from 87.8% to 85.8%). However, in alkaline region, the adsorption efficiency decreased very quickly (down to 3.7% at pH = 10.0). The influence of pH can be explained as follows: The PZC value of IFMB is 6.76. At low pH range, below PZC, the surface of the material is positively charged, favorable for the diffusion and adsorption of anionic R-SO₃⁻ groups in RY-145 molecule under the effect of electrostatic attraction. On the other hand, the higher the pH, the more OH⁻ ions, a negatively charged surface of the material greatly hindered the adsorption process of anions, causing a sharp decrease in efficiency [24–33].

The removal of dyes from water in the presence of nZVI can occur by various mechanisms. The interaction between the dyes and the materials depends mainly on the composition, surface characteristics of the material and solution pH [20–34]. For a better understanding the RY-145 removal mechanism of IFMB, COD and TOC of the solution were measured before and after the adsorption. The results showed that removal efficiency of RY-145 calculated from COD and TOC values is only about 10% lower than that assessed by UV-Vis colorimetry. Moreover, the loss of RY-145 after an adsorption–desorption cycle was determined only 3.2%. Furthermore, observing the UV-Vis spectra as

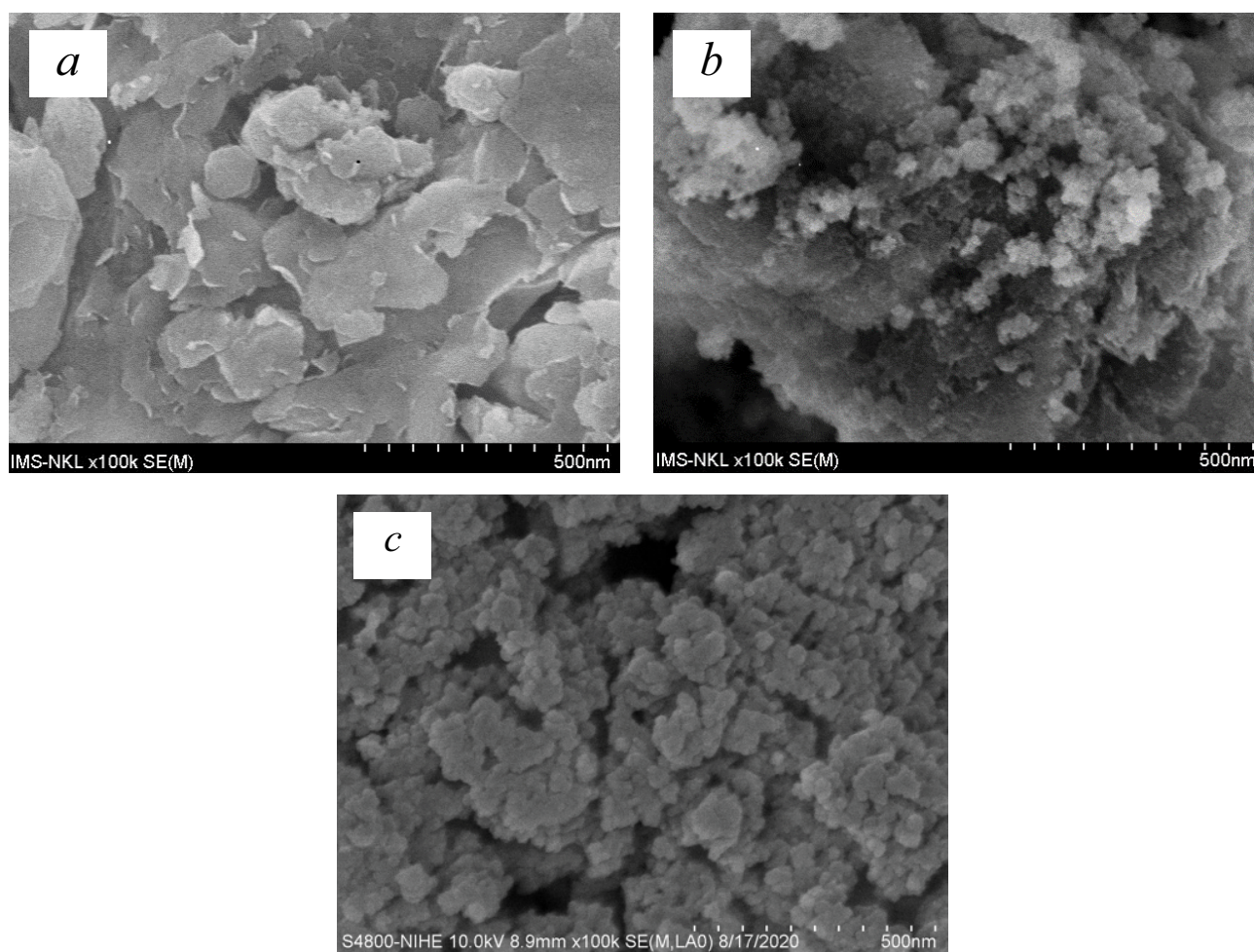


Fig. 2. SEM images of the exfoliated bentonite (a), FMB (b) and (c) IFMB samples.

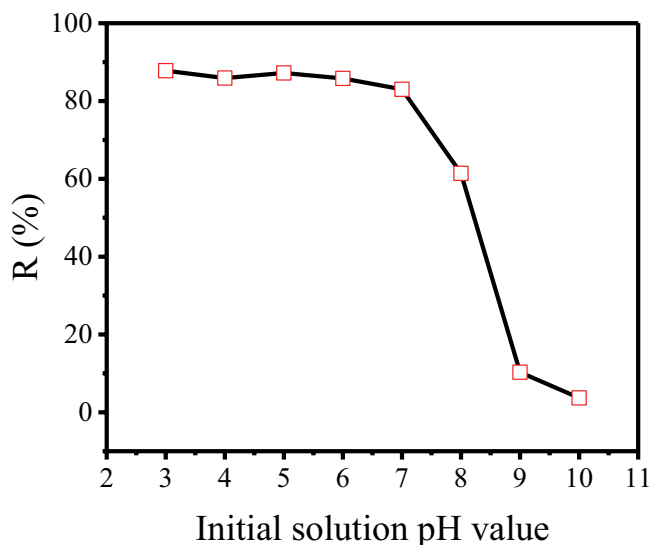


Fig. 3. Effect of pH on the removal efficiency of RY-145 ($C_o = 300 \text{ mg}\cdot\text{L}^{-1}$; IFMB $1.0 \text{ g}\cdot\text{L}^{-1}$; 30°C).

a function of contact time (Fig. 4), there was no abnormal changes found, the spectral shape was almost unchanged during the adsorption.

All of the above data has proved that during the treatment process, RY-145 was hardly decomposed or the oxidation-reduction reactions yielding organic intermediates in solution can be negligible. It can be therefore confirmed that the RY-145 decolorization mechanism of IFMB is predominantly due to the adsorption process.

The adsorption efficiency was quite stable in the pH region below PZC of IFMB and suddenly decreased when the pH was above this value, suggesting that the adsorption mechanism is mainly electrostatic attraction.

3.3. Adsorption kinetics

The results of the adsorption kinetics experiments for IFMB, FMB and nZVIB are displayed in Fig. 5. The adsorption efficiency and rate of RY-145 decreased in the order: IFMB > nZVIB > FMB. For IFMB and nZVIB, the adsorption was very quickly in the first 5 min of contact time (56.4% and 46.5%, respectively) then gradually decreased and reached equilibrium after about 40 min. FMB has the lowest adsorption rate and efficiency, adsorption equilibrium is achieved after 80 min. At equilibrium time, the adsorption efficiency on IFMB was the highest, although the specific surface area of IFMB was lower than that of FMB (218.37 and $283.45 \text{ m}^2\cdot\text{g}^{-1}$, respectively).

It is not surprising that the adsorption rate and efficiency of nZVIB and FMB were different because of completely different nature of these two materials. The interesting point is that there is just about 16% nZVI in IFMB composition, but its adsorption capacity was significantly higher than that of both nZVIB and FMB. This result can be explained only through the “synergistic” effect of FMO, nZVI and bentonite in IFMB composite.

The adsorption kinetic data was analyzed using the pseudo-first-order and pseudo-second-order kinetic models.

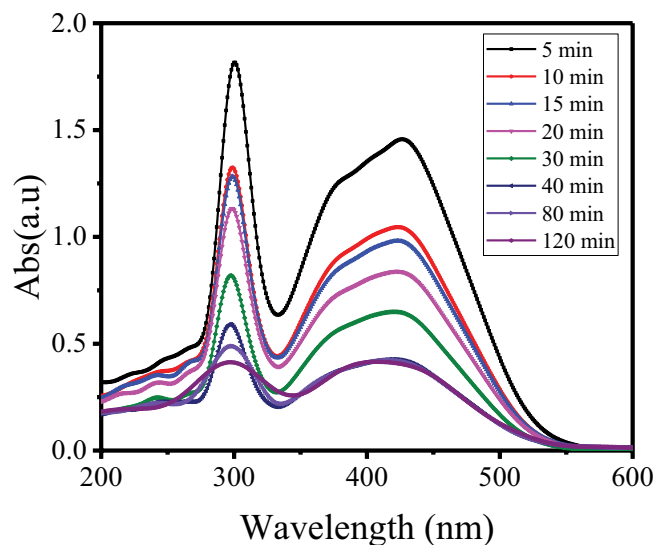


Fig. 4. UV-Vis spectra of RY-145 solution as a function of contact time ($C_o = 300 \text{ mg}\cdot\text{L}^{-1}$; IFMB $1.0 \text{ g}\cdot\text{L}^{-1}$; pH = 6.0; 30°C).

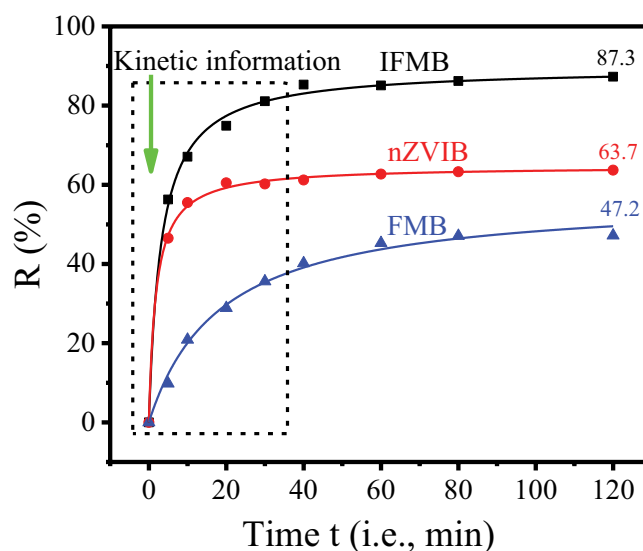


Fig. 5. The plots of RY-145 removal efficiency as function of contact time ($C_o = 300 \text{ mg}\cdot\text{L}^{-1}$; IFMB $1.0 \text{ g}\cdot\text{L}^{-1}$; pH = 6.0; 30°C).

The linear plots of the two models are presented in Fig. 6 and calculated parameters were listed in Table 1. Correlation coefficients R^2 and the comparison of $q_{e,\text{exp}}$ and $q_{e,\text{cal}}$ indicate that the kinetic data was better described by the pseudo-second-order model.

3.4. Adsorption isotherms

Adsorption isotherm data was fitted using Langmuir and Freundlich models (Fig. 7b–d and Table 2). According the higher correlation coefficient R^2 and lower red- χ^2 , the two parameter models of adsorption isotherm Langmuir and D–R model well fitted to the experimental data of adsorption equilibrium compared to the parameter models Freundlich. Nonetheless the parameter

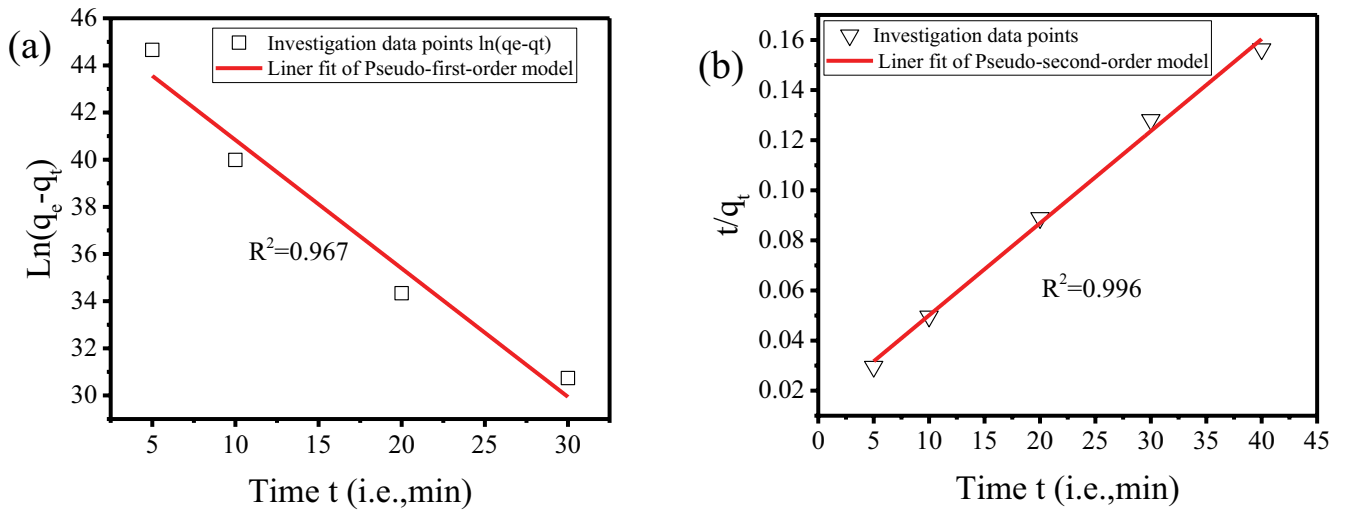


Fig. 6. Pseudo-first-order (a) and pseudo-second-order (b) kinetic plots for RY-145 adsorption on IFMB.

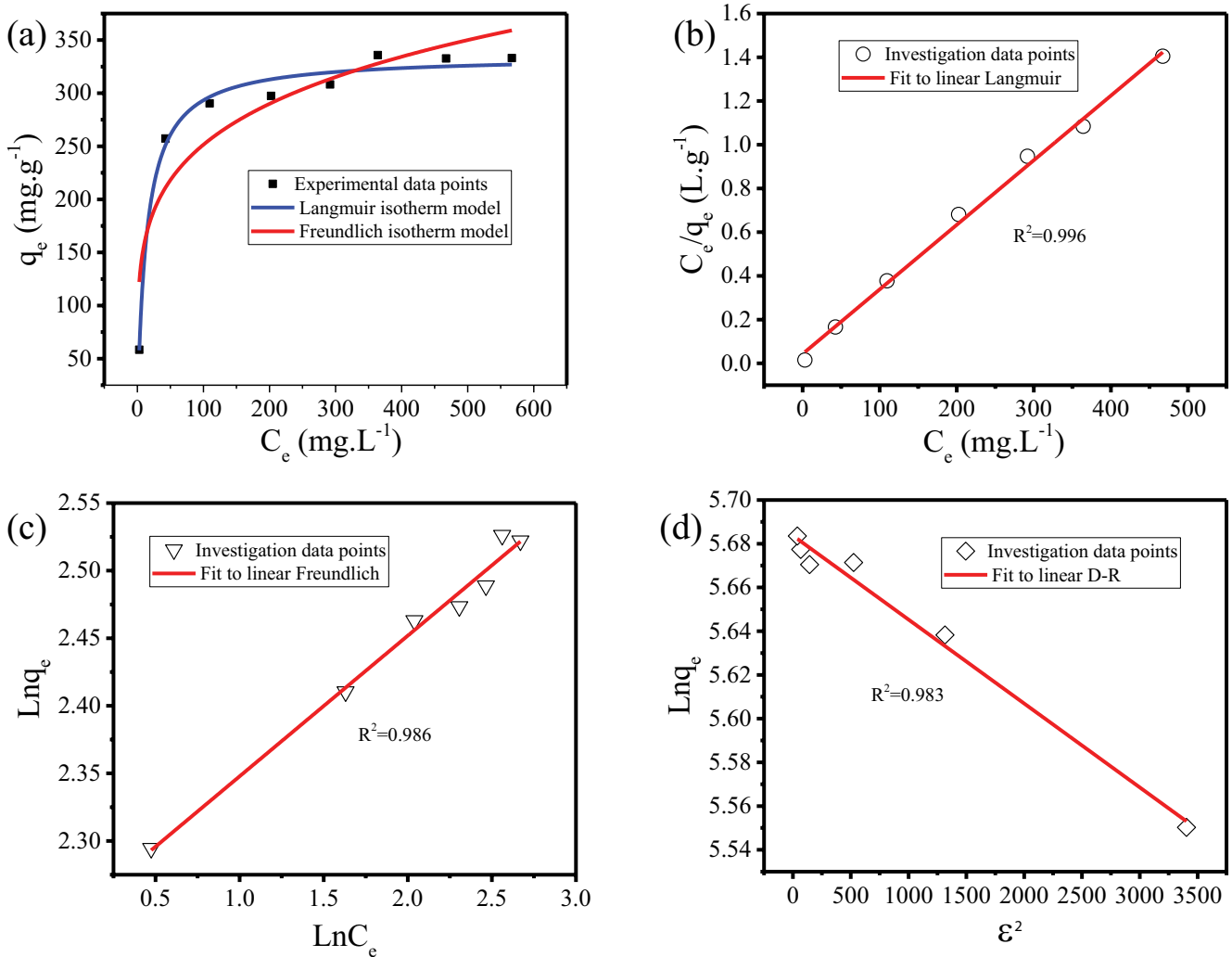


Fig. 7. Adsorption isotherm (a) and linear plots of Langmuir (b), Freundlich (c) and D-R (d) isotherm for RY-145 adsorption on IFMB (IFMB 1.0 g.L^{-1} ; pH = 6.0; 30°C).

Q_{\max} of the Langmuir model is more consistent with the experimental data in Fig. 7a. The adsorption isotherm data was fitted well to Langmuir isotherm model (shown by the correlation coefficient R^2). That proves that IFMB has a relatively homogeneous surface and RY-145 was monolayer-adsorbed. The maximum adsorption capacity, according to Langmuir model, was of 338.9 mg·g⁻¹. This value is relatively high in comparison to that of recently reported materials (Table 3).

3.5. Reusability of IFMB

Comparing XRD patterns of IFMB as prepared and after cycles of adsorption–desorption (Fig. 8a), there is no change in phase composition and no new crystalline phases appeared, showing that nZVI phase and Mn–Fe complex oxide in the composite material are relatively stable, not converted into other crystalline oxides. However, the intensity of characterized peaks of nZVI gradually decreased with the number of cycles, indicating a loss of

Table 1
Kinetic parameters for RY-145 adsorption on IFMB ($C_o = 300 \text{ mg}\cdot\text{L}^{-1}$; IFMB $1.0 \text{ g}\cdot\text{L}^{-1}$; pH = 6.0; 30°C)

Model	RY-145
Pseudo-first-order kinetic model	
C_o	300.0
$q_{e,\text{exp}}$	255.81
k_1	1.226
$q_{e,\text{cal}}$	102.40
adj- R^2	0.967
red- χ^2	0.951
Pseudo-second-order kinetic model	
C_o	300.0
$q_{e,\text{exp}}$	255.81
k_2	0.001
$q_{e,\text{cal}}$	270.0
adj- R^2	0.996
red- χ^2	0.994

Adjusted coefficient of determination R^2 and the reduced chi-square statistic (red- χ^2).

Table 3
Comparison of adsorption capacities of various adsorbents for RY-145

Adsorbent	T (°C)	pH	C_o (mg·L ⁻¹)	Q_{\max} (mg·g ⁻¹)	Isotherm model	References
Chitosan-coated magnetite nanoparticle (Fe ₃ O ₄ -CS)	25	3.0	50–200	47.60	Langmuir	[35]
Activated carbon from Iraqi kehdrawy date palm seeds	25	5.5	–	9.79	Langmuir	[36]
Bentonite modified with L-proline-epichlorohydrin polymer (Pro-Ben)	25	5.2	–	78.56	Langmuir	[37]
CTS/MMT	50	3.0	50–400	363.33	Langmuir	[38]
Textile sludge-based activated carbon (TSBAC)	–	3.0	50–400	125.00	Langmuir	[39]
IFMB	30	6.0	200–900	338.9	Langmuir	This work

nZVI (possibly because the material was gradually dissolved in each period). This is also consistent with the adsorption results given in Fig. 8b, after 5 cycles RY-145 adsorption efficiency decreased from 85.7% to 63.8%. In practice, despite this degree of reduction, the IFMB can still be reused many times with the desired efficiency.

4. Conclusion

A novel (nZVI/Fe–Mn) binary oxide/bentonite (IFMB) nanocomposite, developed in our study, exhibits a good performance for the removal of RY-145 dye from aqueous solution.

The RY-145 removal mechanism of IFMB material is mainly due to the adsorption process, which takes place predominantly by electrostatic attraction.

The adsorption of RY-145 on IFMB is strongly dependent on the pH of solution. The adsorption efficiency was high and relatively stable in the pH range from 3.0 to 7.0.

Table 2
Langmuir, Freundlich and D–R parameters for RY-145 adsorption on IFMB

Model	RY-145
Langmuir model	
Q_{\max}	338.9
K_L	0.0689
adj- R^2	0.996
red- χ^2	0.995
Freundlich model	
K_F	175.39
n	9.61
adj- R^2	0.986
red- χ^2	0.982
D–R model	
Q_{\max}	294.03
K_{DR}	3.84×10^{-5}
Energy of adsorption	114.11
adj- R^2	0.986
red- χ^2	0.983

Adjusted coefficient of determination R^2 and the reduced chi-square statistic (red- χ^2).

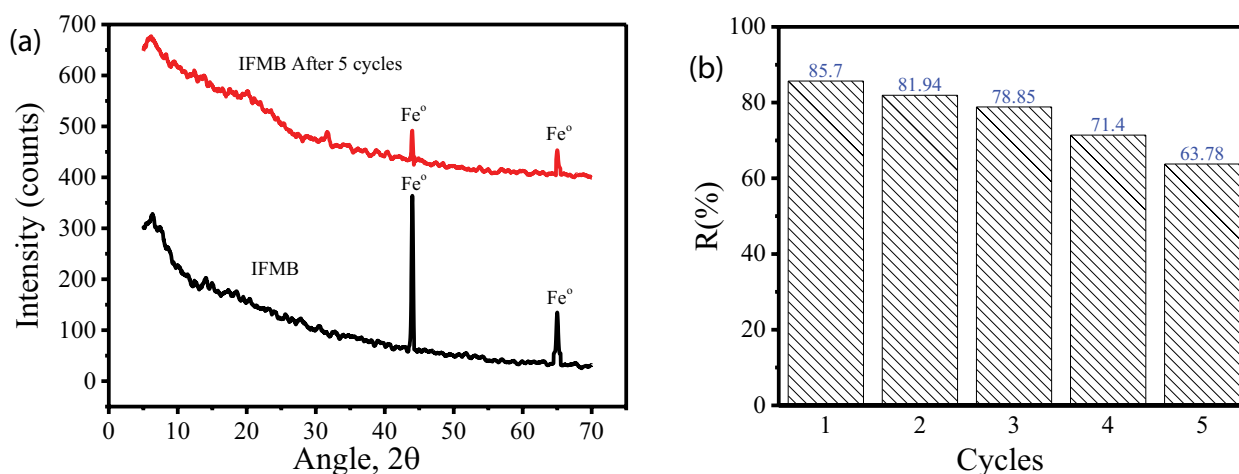


Fig. 8. (a) XRD patterns of IFMB as-prepared and after 5 cycles of adsorption–desorption and (b) adsorption–desorption cycles of RY-145 on IFMB.

The experimental results indicated the “synergistic” interaction between FMO, nZVI and bentonite existed in the composite has enhanced significantly both of the adsorption rate and efficiency for RY-145. The adsorption kinetics was fitted well to a pseudo-second-order kinetics model and the adsorption reached equilibrium after contact time of about 40 min. The adsorption isotherms agreed well with the Langmuir model with a maximum adsorption capacity of 338.9 mg·g⁻¹.

Future research should be carried out in azo dye containing wastewater in order to confirm the application potential of IFMB in practice.

Acknowledgments

The authors thanks the Vietnam Academy of Science and Technology for financial support of this work (VAST07.01/20-21).

References

- [1] S. Benkhaya, S. M'rabet, A. El Harfi, Classifications, properties, recent synthesis and applications of azo dyes, *Heliyon*, 6 (2020) e03271, doi: 10.1016/j.heliyon.2020.e03271.
- [2] S. Dutta, R. Saha, H. Kalita, A.N. Bezbaruah, Rapid reductive degradation of azo and anthraquinone dyes by nanoscale zero-valent iron, *Environ. Technol. Innovation*, 5 (2016) 176–187.
- [3] A. Mehrizad, M.A. Behnajady, P. Gharbani, S. Sabbagh, Sonocatalytic degradation of Acid Red 1 by sonochemically synthesized zinc sulfide-titanium dioxide nanotubes: optimization, kinetics and thermodynamics studies, *J. Cleaner Prod.*, 215 (2019) 1341–1350.
- [4] M.T. Yagub, T.K. Sen, S. Afroze, H.M. Ang, Dye and its removal from aqueous solution by adsorption: a review, *Adv. Colloid Interface Sci.*, 209 (2014) 172–184.
- [5] M.A. Islam, I. Ali, S.M.A. Karim, M.S. Hossain Firoz, A.-N. Chowdhury, D.W. Morton, M.J. Angove, Removal of dye from polluted water using novel nano manganese oxide-based materials, *J. Water Process Eng.*, 32 (2019) 100911, doi: 10.1016/j.jwpe.2019.100911.
- [6] E. Fathi, P. Gharbani, Modeling and optimization removal of reactive Orange 16 dye using MgO/g-C₃N₂/zeolite nanocomposite in coupling with LED and ultrasound by response surface methodology, *Diamond Relat. Mater.*, 115 (2021) 108346, doi: 10.1016/j.diamond.2021.108346.
- [7] P. Xu, G. Ming Zeng, D.L. Huang, C.L. Feng, S. Hu, M.H. Zhao, C. Lai, Z. Wei, C. Huang, G.X. Xie, Z.F. Liu, Use of iron oxide nanomaterials in wastewater treatment: a review, *Sci. Total Environ.*, 424 (2012) 1–10.
- [8] I. Polowczyk, P. Cyganowski, J. Ulatowska, W. Sawiński, A. Bastrzyk, Synthetic iron oxides for adsorptive removal of arsenic, *Water Air Soil Pollut.*, 229 (2018) 203, doi: 10.1007/s11270-018-3866-2.
- [9] K. Lu, T. Wang, L. Zhai, W. Wu, S. Dong, S. Gao, L. Mao, Adsorption behavior and mechanism of Fe–Mn binary oxide nanoparticles: adsorption of methylene blue, *J. Colloid Interface Sci.*, 539 (2019) 553–562.
- [10] G. Zhang, J. Qu, H. Liu, R. Liu, R. Wu, Preparation and evaluation of a novel Fe–Mn binary oxide adsorbent for effective arsenite removal, *Water Res.*, 41 (2007) 1921–1928.
- [11] G.-S. Zhang, J.-H. Qu, H.-J. Liu, R.-P. Liu, G.-T. Li, Removal mechanism of As(III) by a novel Fe–Mn binary oxide adsorbent: oxidation and sorption, *Environ. Sci. Technol.*, 41 (2007) 4613–4619.
- [12] M. Liang, S. Xu, Y. Zhu, X. Chen, Z. Deng, L. Yan, H. He, Preparation and Characterization of Fe–Mn binary oxide/mulberry stem biochar composite adsorbent and adsorption of Cr(VI) from aqueous solution, *Int. J. Environ. Res. Public Health*, 17 (2020) 676, doi: 10.3390/ijerph17030676.
- [13] G. Yin, X. Song, L. Tao, B. Sarkar, A.K. Sarmah, W. Zhang, Q. Lin, R. Xiao, Q. Liu, H. Wang, Novel Fe–Mn binary oxide-biochar as an adsorbent for removing Cd(II) from aqueous solutions, *Chem. Eng. J.*, 389 (2020) 124465, doi: 10.1016/j.cej.2020.124465.
- [14] Q. Ning, Z. Yin, Y. Liu, X. Tan, G. Zeng, L. Jiang, S. Liu, S. Tian, N. Liu, X. Wang, Fabrication of stabilized Fe–Mn binary oxide nanoparticles: effective adsorption of 17β-estradiol and influencing factors, *Int. J. Environ. Res. Public Health*, 15 (2018) 2218, doi: 10.3390/ijerph15102218.
- [15] L.-B. Zhong, J. Yin, S.-G. Liu, Q. Liu, Y.-S. Yang, Y.-M. Zheng, Facile one-pot synthesis of urchin-like Fe–Mn binary oxide nanoparticles for effective adsorption of Cd(II) from water, *RSC Adv.*, 6 (2016) 103438–103445.
- [16] R.A. Crane, T.B. Scott, Nanoscale zero-valent iron: future prospects for an emerging water treatment technology, *J. Hazard. Mater.*, 211 (2012) 112–125.
- [17] C.D. Raman, S. Kanmani, Textile dye degradation using nano zero valent iron: a review, *J. Environ. Manage.*, 177 (2016) 341–355.
- [18] R. Mukherjee, R. Kumar, A. Sinha, Y. Lama, A.K. Saha, A review on synthesis, characterization, and applications of nano zero valent iron (nZVI) for environmental remediation, *Crit. Rev. Env. Sci. Technol.*, 46 (2016) 443–466.

- [19] D. O'Carroll, B. Sleep, M. Krol, H. Boparai, C. Kocur, Nanoscale zero valent iron and bimetallic particles for contaminated site remediation, *Adv. Water Resour.*, 51 (2013) 104–122.
- [20] T. Pasinszki, M. Krebsz, Synthesis and application of zero-valent iron nanoparticles in water treatment, environmental remediation, catalysis, and their biological effects, *Nanomaterials* (Basel), 10 (2020) 917, doi: 10.3390/nano10050917.
- [21] N.A. Zarime, W.Z.W. Yaacob, H. Jamil, Decolourization of anionic dye by activated carbon-supported nano-zero valent iron (nZVI), *Chem. Eng. Trans.*, 73 (2019) 85–90.
- [22] A.D. Bokare, R.C. Chikate, C.V. Rode, K.M. Paknikar, Iron-nickel bimetallic nanoparticles for reductive degradation of azo dye Orange G in aqueous solution, *Appl. Catal., B*, 79 (2008) 270–278.
- [23] M. Barreto-Rodrigues, J. Silveira, J.A. Zazo, J.J. Rodriguez, Synthesis, characterization and application of nanoscale zero-valent iron in the degradation of the azo dye Disperse Red 1, *J. Environ. Chem. Eng.*, 5 (2017) 628–634.
- [24] D.V. Kerkez, D.D. Tomašević, G. Kozma, M.R. Bečelić-Tomin, M.D. Prica, S.D. Rončević, Á. Kukovec, B.D. Dalmacija, Z. Kónya, Three different clay-supported nanoscale zero-valent iron materials for industrial azo dye degradation: a comparative study, *J. Taiwan Inst. Chem. Eng.*, 45 (2014) 2451–2461.
- [25] H. Thanh, D. Binh, T. Thu, B. Ngoc, L. Van, Preparation and optimization of the composition of novel nZVI/(Fe–Mn) binary oxide/bentonite adsorbent for removal of Reactive Yellow 145 dye (RY-145) from aqueous solution, *JCA*, 9 (2020) 45–51.
- [26] G. Zhang, H. Liu, J. Qu, W. Jefferson, Arsenate uptake and arsenite simultaneous sorption and oxidation by Fe–Mn binary oxides: influence of Mn/Fe ratio, pH, Ca²⁺, and humic acid, *J. Colloid Interface Sci.*, 366 (2012) 141–146.
- [27] Ç. Üzümlü, T. Shahwan, A.E. Eroğlu, I. Lieberwirth, T.B. Scott, K.R. Hallam, Application of zero-valent iron nanoparticles for the removal of aqueous Co²⁺ ions under various experimental conditions, *Chem. Eng. J.*, 144 (2008) 213–220.
- [28] C.R. Keenan, R. Goth-Goldstein, D. Lucas, D.L. Sedlak, Oxidative stress induced by zero-valent iron nanoparticles and Fe(II) in human bronchial epithelial cells, *Environ. Sci. Technol.*, 43 (2009) 4555–4560.
- [29] Y. Wu, M. Yang, S. Hu, L. Wang, H. Yao, Characteristics and mechanisms of 4A zeolite supported nanoparticulate zero-valent iron as Fenton-like catalyst to degrade methylene blue, *Toxicol. Environ. Chem.*, 96 (2014) 227–242.
- [30] Y.S. Ho, G. McKay, Pseudo-second-order model for sorption processes, *Process Biochem.*, 34 (1999) 451–465.
- [31] J. Wang, G. Liu, T. Li, C. Zhou, Physicochemical studies toward the removal of Zn(II) and Pb(II) ions through adsorption on montmorillonite-supported zero-valent iron nanoparticles, *RSC Adv.*, 5 (2015) 29859–29871.
- [32] M.A. Al-Ghouti, D.A. Da'ana, Guidelines for the use and interpretation of adsorption isotherm models: a review, *J. Hazard. Mater.*, 393 (2020) 122383, doi: 10.1016/j.jhazmat.2020.122383.
- [33] P. Gharbani, Modeling and optimization of Reactive Yellow 145 dye removal process onto synthesized MnO_x–CeO₂ using response surface methodology, *Colloids Surf., A*, 548 (2018) 191–197.
- [34] F. Freyria, S. Esposito, M. Armandi, F. Deorsola, E. Garrone, B. Bonelli, Role of pH in the aqueous phase reactivity of zerovalent iron nanoparticles with Acid Orange 7, a model molecule of azo dyes, *J. Nanomater.*, 2017 (2017) 1–13.
- [35] N.A. Kalkan, S. Aksoy, E.A. Aksoy, N. Hasirci, Adsorption of Reactive Yellow 145 onto chitosan coated magnetite nanoparticles, *J. Appl. Polym. Sci.*, 124 (2012) 576–584.
- [36] A. Lafta, H. Ismael, N. Nema, S. Kadhim, A. Mousa, K. Abdali, Removal of reactive yellow dye 145 from wastewaters over activated carbon that is derived from Iraqi kehdrawy date palm seeds, *WSN*, 21 (2015) 124–136.
- [37] S. Raghunath, K. Anand, R.M. Gengan, M.K. Nayunigari, A. Maity, Sorption isotherms, kinetic and optimization process of amino acid proline based polymer nanocomposite for the removal of selected textile dyes from industrial wastewater, *J. Photochem. Photobiol., B*, 165 (2016) 189–201.
- [38] J. Li, J. Cai, L. Zhong, H. Wang, H. Cheng, Q. Ma, Adsorption of reactive dyes onto chitosan/montmorillonite intercalated composite: multi-response optimization, kinetic, isotherm and thermodynamic study, *Water Sci. Technol.*, 77 (2018) 2598–2612.
- [39] N. Oke, S. Mohan, Development of nanoporous textile sludge-based adsorbent for the dye removal from industrial textile effluent, *J. Hazard. Mater.*, 422 (2022) 126864, doi: 10.1016/j.jhazmat.2021.126864.